



**HAL**  
open science

# Optical Activity of Spin-Forbidden Electronic Transitions in Metal Complexes from Time-Dependent Density Functional Theory with Spin-Orbit Coupling

Herbert D. Ludowieg, Monika Srebro-Hooper, Jeanne Crassous, Jochen Autschbach

► **To cite this version:**

Herbert D. Ludowieg, Monika Srebro-Hooper, Jeanne Crassous, Jochen Autschbach. Optical Activity of Spin-Forbidden Electronic Transitions in Metal Complexes from Time-Dependent Density Functional Theory with Spin-Orbit Coupling. *ChemistryOpen*, 2022, 11 (5), pp.e202200020. 10.1002/open.202200020 . hal-03688085

**HAL Id: hal-03688085**

**<https://hal.science/hal-03688085>**

Submitted on 6 Apr 2023

**HAL** is a multi-disciplinary open access archive for the deposit and dissemination of scientific research documents, whether they are published or not. The documents may come from teaching and research institutions in France or abroad, or from public or private research centers.

L'archive ouverte pluridisciplinaire **HAL**, est destinée au dépôt et à la diffusion de documents scientifiques de niveau recherche, publiés ou non, émanant des établissements d'enseignement et de recherche français ou étrangers, des laboratoires publics ou privés.



Distributed under a Creative Commons Attribution 4.0 International License

Special  
Collection

# Optical Activity of Spin-Forbidden Electronic Transitions in Metal Complexes from Time-Dependent Density Functional Theory with Spin-Orbit Coupling

Herbert D. Ludowieg,<sup>[a]</sup> Monika Srebro-Hooper,<sup>[b]</sup> Jeanne Crassous,<sup>[c]</sup> and Jochen Autschbach<sup>\*[a]</sup>

The calculation of magnetic transition dipole moments and rotatory strengths was implemented at the zeroth-order regular approximation (ZORA) two-component relativistic time-dependent density functional theory (TDDFT) level. The circular dichroism of the spin-forbidden ligand-field transitions of tris(ethylenediamine)cobalt(III) computed in this way agrees very well with available measurements. Phosphorescence dissymmetry factors  $g_{\text{lum}}$  and the corresponding lifetimes are

evaluated for three N-heterocyclic-carbene-based iridium complexes, two of which contain helicene moieties, and for two platinum-helicenes. The agreement with experimental data is satisfactory. The calculations reproduce the signs and order of magnitude of  $g_{\text{lum}}$ , and the large variations of phosphorescence lifetimes among the systems. The electron spin contribution to the magnetic transition dipole moment is shown to be important in all of the computations.

## Introduction

There is continuing strong interest in the photophysical properties of metal complexes, driven by numerous applications such as electro-emissive switches, luminescent sensors, cellular imaging agents, photosensitizers, and emissive materials for organic light-emitting diode (OLED) technology. Among phosphorescent emitters, Ir(III) compounds with a pseudo-octahedral coordination environment and Pt(II) systems with square-planar structures have emerged as particularly appealing and thus have been developed and examined extensively.<sup>[1–4]</sup> For example, Ir(ppy)<sub>3</sub> (ppy = 2-phenylpyridine) has been studied intensely by theory and experiment in the context of developing complexes with strong emission in different parts of the visible spectrum.<sup>[5–15]</sup>

Chiral enantiopure systems give access not only to desired emission wavelengths, but also the ability to modulate circularly polarized (CP) luminescence (CPL).<sup>[16–19]</sup> Strong optical activity of metal complexes can be obtained, in particular, when not only the relative arrangement of the ligands is chiral, but when the ligands themselves are inherently chiral and display strong optical activity themselves. Helicenes play a particularly important role in this context.<sup>[20–22]</sup> For example, chiral Ir(III) complexes with a pentahelicenic N-heterocyclic carbene (NHC) ligand such as  $(P, \Lambda_{\text{Ir}})\text{-A}^1$  and  $(P, \Lambda_{\text{Ir}})\text{-A}^2$  (Figure 1; note that the systems are diastereoisomers differing in absolute configuration at the metal center) reported in Ref. [23] have shown promise as chiral dopants in CP-OLEDs and singlet-oxygen sensitizers, among other applications,<sup>[17,24–26]</sup> because they displayed very long-lived CP blue-green phosphorescence. The emission lifetimes were increased by a factor of 100, and the sign of the CPL signal was controlled by the stereochemistry of the  $\pi$ -helical NHC ligand, in comparison to the non-helicenic NHC model complex  $\Lambda_{\text{Ir}}\text{-A}$ . Another very interesting class of chiral systems combining

[a] H. D. Ludowieg, Prof. J. Autschbach  
Department of Chemistry  
University at Buffalo  
State University of New York  
Buffalo, NY-14260-3000 (USA)  
E-mail: jochena@buffalo.edu

[b] Prof. M. Srebro-Hooper  
Faculty of Chemistry  
Jagiellonian University  
Gronostajowa 2  
30-387, Krakow (Poland)

[c] Dr. J. Crassous  
Université Rennes  
CNRS, ISCR – UMR 6226  
35000 Rennes (France)

Supporting information for this article is available on the WWW under <https://doi.org/10.1002/open.202200020>

An invited contribution to a Special Collection dedicated to the latest research of ChemistryOpen's Editorial Advisory Board Members.

© 2022 The Authors. Published by Wiley-VCH GmbH. This is an open access article under the terms of the Creative Commons Attribution License, which permits use, distribution and reproduction in any medium, provided the original work is properly cited.

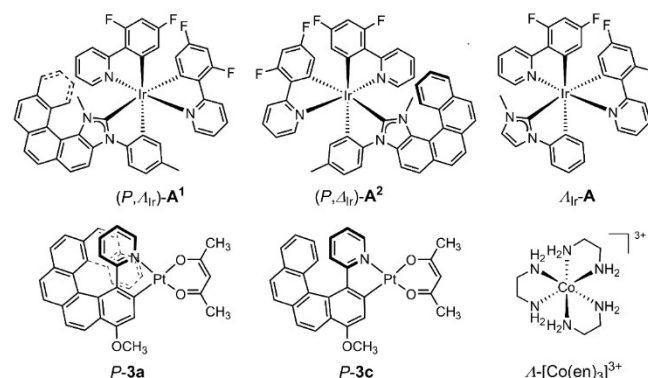


Figure 1. Metal complexes studied in this work.

metal centers and helicene moieties are platinahelicenes.<sup>[27–32]</sup> Chemical formulas for two representative systems from Ref. [30], platina[8]helicene *P-3a* and platina[6]helicene *P-3c*, are shown in Figure 1. Here, the metal atom is part of the helical  $\pi$ -system of the chromophore, leading to room-temperature CP phosphorescence, and useful redox activity, among other desirable properties. Importantly, *P-3c* was utilized to prepare the first helicene-based CP-OLED shown to yield high electrophosphorescence.<sup>[17]</sup>

Long-lived phosphorescence is associated with spin-forbidden radiative electronic transitions to the ground state. Spin-orbit coupling (SOC), a relativistic effect<sup>[33]</sup> generated in the electronic structure by the presence of the high nuclear charge of the heavy metal, is responsible for lifting the spin selection rule, such that these transitions become weakly allowed. For the rational development of CP emitters, it is very important that their physico-chemical properties can be predicted and analyzed with the help of quantum-chemical theoretical methods. The most important parameters are the oscillator or dipole strength ( $f$  or  $D$ ), and the phosphorescence lifetime  $\tau$  or rate  $k = 1/\tau$  for the spin-forbidden transition. For CP emitters, in addition to the phosphorescence quantum yields and lifetimes, the rotatory strength  $R$  and the luminescence dissymmetry factor  $g_{\text{lum}} = 2(I_L - I_R)/(I_L + I_R)$  are the key parameters pertaining to the optical activity of the emission.

A popular wavefunction theory approach for calculating excited-state properties and transition moments is based on the complete active space (CAS) self-consistent field (SCF) method and its variants and extensions,<sup>[34]</sup> with treatment of SOC via state interaction, as implemented, for example, in the Orca<sup>[35]</sup> and Molcas programs.<sup>[36]</sup> Such calculations have been performed in the context of the optical activity of metal complexes such as *P-3c* and the  $D_3$  symmetric benchmark systems [Co(en)<sub>3</sub>]<sup>3+</sup> and tris(DPA)europium(III) (en = ethylenediamine = 1,2-diaminoethane, DPA = (2,6)-pyridinedicarboxylate).<sup>[30,37]</sup> However, some difficulties were noted regarding the size of the active space required to obtain reliable intensities, and the scaling of CASSCF-based methods with the system size and active space is unfavorable. A less demanding correlated wavefunction approach is the approximate coupled-cluster with singles and doubles method called CC2, for which CP luminescence calculations for organic molecules have been reported.<sup>[38]</sup> For larger systems, time-dependent density functional theory (TDDFT), in particular in its response framework, remains the method of choice for most practical applications in photochemistry,<sup>[39–42]</sup> including optical activity<sup>[43,44]</sup> and specifically including CP luminescence.<sup>[45,46]</sup> With certain approximations and simplifications,<sup>[47,48]</sup> even very large molecules and molecular aggregates can be targeted. A recent study<sup>[49]</sup> reported a series of calculations of the spin-allowed vibronic electronic circular dichroism (ECD) and one-photon vibrationally resolved absorption and emission spectra of the iridium complexes of Figure 1, underlining the interest in such systems as well as pointing out the lack of reliable relativistic methods for spin-forbidden CP computations for these types of compounds. Spin-forbidden CP emission of some organic molecules was determined in Ref. [50] from TDDFT calculations that

treated SOC as a linear perturbation. For systems with heavy atoms such as the ones shown in Figure 1, this level of treating SOC is unlikely to be sufficient. For example, inspection of the formalism does not indicate that there are electron spin contributions to the magnetic transition dipole moments entering the rotatory strengths. Two-component relativistic TDDFT (2c-TDDFT) approaches for treating spin-forbidden transitions and phosphorescence lifetimes with SOC included variationally are also available, and were demonstrated to be applicable to complexes with heavy metals of the size that would be of interest in CP-OLED applications.<sup>[11,51–53]</sup> In particular, Mori et al.<sup>[10]</sup> demonstrated applicability of the method of Ref. [51] to calculate phosphorescence lifetimes and the  $T_1$  state zero-field splitting for a large variety of organometallic complexes.

For the purpose of studying the photophysical properties, and specifically the CP luminescence, of heavy metal complexes, we extended the efficient 2c-TDDFT code used by Mori et al.,<sup>[10]</sup> to calculate also the rotatory strengths of the transitions, a feature not previously available in this program. We then applied it to the systems shown in Figure 1. These complexes have been characterized experimentally previously, and TDDFT calculations of the spin-allowed ECD were shown to match well with measured data.<sup>[23,27,28,30]</sup> However, it was not possible to support the experimental characterizations of the CP phosphorescence fully by calculations. The present study aims to fill this gap. In particular, we show that the calculated  $g_{\text{lum}}$  of *P-3c* is consistent with a revised experimental value that differs considerably from the one reported in Ref. [30]. Furthermore, electron spin contributions to the magnetic transition moments are shown to be responsible for the positive signs of  $g_{\text{lum}}$  of complexes *P-3a* and *P-3c*. In addition to the emission data of the Ir and Pt complexes in Figure 1, we also investigate the ECD of the ligand-field (LF) transitions of tris(ethylenediamine)cobalt(III) ( $\Lambda$ -[Co(en)<sub>3</sub>]<sup>3+</sup>). An experimental spectrum, including the weakly intense triplet excitations at low energy, is available,<sup>[54]</sup> and spin-allowed natural electronic optical activity of the complex has been studied extensively in the past using TDDFT methods,<sup>[55–57]</sup> rendering it a suitable system to benchmark new theoretical methods for the optical activity of metal complexes.

## Theory

The formalism outlined in the following was implemented in the 2019 version of the Amsterdam Density Functional (ADF) program,<sup>[58]</sup> and in a 2021 developer's version of ADF. All-electron relativistic computations were based on the two-component zeroth-order regular approximation (ZORA) Hamiltonian<sup>[59]</sup> and Slater-type orbital (STO) basis sets optimized for ZORA calculations,<sup>[60]</sup> as specified in the Computational Section. Excitation energies and transition moments were computed with the 'Excitations' module of ADF.<sup>[51,61]</sup> The calculation of rotatory strengths of spin-allowed transitions, using the dipole-length and dipole-velocity gauges, with the latter being origin invariant by construction, was previously implemented in ADF by one of us.<sup>[55]</sup> For the present study, the

functionality of the 2c-TDDFT module in ADF was extended in a similar way to determine the dipole-velocity in addition to the dipole-length electric transition dipole moment, as well as the magnetic transition dipole moment  $\mathbf{m} = \langle 0|\hat{\mathbf{m}}|j\rangle$ , between the ground state (0) and an excited state ( $j$ ). The electron magnetic moment operator is  $\hat{\mathbf{m}} = -\mu_B(\hat{\mathbf{L}} + 2\hat{\mathbf{S}})$ . The constant  $\mu_B$  is the Bohr magneton, and  $\hat{\mathbf{L}}$  and  $\hat{\mathbf{S}}$  are dimensionless electron orbital and spin angular momentum vector operators, respectively. The magnetic moment operator is therefore in the 'nonrelativistic with spin' form and, like the electric dipole moment, not corrected for relativistic picture change. The nonrelativistic with spin form of the magnetic operator is heavily used for theoretical work in molecular magnetism<sup>[62]</sup> and related fields, indicating that it is a good approximation for valence states. With the corresponding electric transition dipole moment  $\mathbf{d}$ , the dipole and rotatory strength are [Eq. (1)]:

$$D = \mathbf{d} \cdot \mathbf{d}^* ; R = \text{Im}[\mathbf{d} \cdot \mathbf{m}^*] \quad (1)$$

In cgs-based Gaussian units, the dipole and rotatory strengths have the same unit of  $\text{esu}^2\text{cm}^2$ . Using these units, the dissymmetry factor for the transition is given by:

$$g_{\text{lum}} = 4R/D \quad (2)$$

For a parity-forbidden transition,  $D$  should be generalized to include terms from the multipole expansion of the transition probability beyond the electric dipole.<sup>[37]</sup> For the present study, this was deemed unnecessary.

The radiative decay rate constant  $k$  for a transition was calculated according to Equation 2 in the study of Mori et al.,<sup>[10]</sup> which we reformulate here in terms of the oscillator strength as:

$$k = 2\alpha^3 n^2 E^2 f \quad (3)$$

In Equation (3),  $f = (2/3)ED$  is the dimensionless oscillator strength, with  $E$  and  $D$  being the transition energy and dipole strength in Hartree atomic units, respectively,  $\alpha$  is the fine structure constant, and  $n$  is the refractive index of the medium. In the calculations,  $n=1.42$  was chosen, representing the dichloromethane solvent used in the measurements.

The lowest spin triplet states of the examined Pt and Ir complexes exhibit weak zero-field splitting. The rate constants  $k_i$  for the individual components of the  $T_1$  state were Boltzmann averaged, following Mori et al.,<sup>[10]</sup> at room temperature (298 K). The averaged radiative lifetime  $\tau = 1/k$  was then calculated based on the Boltzmann-averaged rate constant and converted from atomic units to  $\mu\text{s}$ . In a similar fashion, an averaged dissymmetry factor for the emission was computed based on Equation (2) using rotatory and dipole strengths that were Boltzmann-averaged over the triplet components.

Computational details are provided in a separate section near the end of the article.

## Results and Discussion

### Tris(ethylenediamine)cobalt(III)

See the Computational Section regarding the structure nomenclature *ob* and *lel* and a description of test calculations that were performed for the different conformers with different functionals. We focus here on the results for the *lel*<sub>3</sub> conformer obtained with 2c-TDDFT, the Tamm-Dancoff approximation (TDA), and the PBE0 hybrid functional. The calculated ligand-field ECD spectrum of *lel*<sub>3</sub>- $\Lambda$ -[Co(en)<sub>3</sub>]<sup>3+</sup> is displayed in Figure 2 and compared to the experimental spectrum recorded in aqueous solution by Mason and Peart.<sup>[54]</sup> Additional computed data for  $\Lambda$ -[Co(en)<sub>3</sub>]<sup>3+</sup> can be found in the Supporting Information. The *lel*<sub>3</sub> conformer has  $D_3$  symmetry. The distortion of the coordinating nitrogen atoms from  $O_h$  parent symmetry is not very large, such that the spectroscopic properties can be discussed either in terms of the  $D_3$  or the parent  $O_h$  symmetry species. Cobalt(III) is a  $3d^6$  ion. The complex is low spin, with a filled 3d  $t_{2g}$  sub-shell. The LF transitions are therefore  $t_{2g}$  to  $e_g$ , with excited states of symmetry  $T_1$  and  $T_2$ . Distorting the symmetry to  $D_3$  causes the  $t_{2g}$  orbital set to split into  $a_1$  and  $e$  species. The corresponding  $T_1$  excited LF state splits into  $A_2$  and  $E$  components, whereas the  $T_2$  excited state splits into  $A_1$  and  $E$ . The transitions from the  $A_1$  ground state to the  $A_2$  and  $E$  excited states become electric dipole allowed. The two  $E$ -symmetric LF states have been conveniently distinguished as  $E_a$  (from  $T_1$ ) and  $E_b$  (from  $T_2$ ).<sup>[54]</sup>

The non-magnified portion of the spectra shown in Figure 2 is from the singlet excitations. Based on additional absorption and ECD measurements for a crystal, with different orientation relative to the light polarization/propagation, Mason and Peart<sup>[54]</sup> assigned the pair of singlet bands between  $20$  and  $25 \times 10^3 \text{ cm}^{-1}$  to the split  $T_1$  state, with  $E_a$  (positive  $R$ ) at lower energy and  $A_2$  (negative  $R$ ) at higher energy, and the band close to  $30 \times 10^3 \text{ cm}^{-1}$  as  $T_2/E_b$ . The first TDDFT calculations of the ECD spectra,<sup>[63]</sup> in 2003, confirmed the assignment. However, with the BP86 non-hybrid functional used in the original computation, the LF excitation wavenumbers were too large by several thousand inverse cm. PBE0 gives much better energies for the

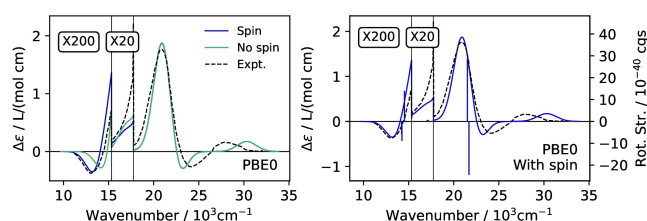


**Figure 2.** Left: ECD spectra for *lel*<sub>3</sub>- $\Lambda$ -[Co(en)<sub>3</sub>]<sup>3+</sup> comparing spin-orbit calculations including (blue, 'Spin') or excluding (green, 'No spin') the electron spin contributions in the magnetic transition dipole moments. 2c-TDDFT calculations used the PBE0 functional along with the TDA in the dipole-length gauge. Right: The 'stick spectrum' represents the electronic excitation energies and rotatory strengths. Both panels: Experimental spectrum digitized from Ref. [54].  $\Delta\epsilon$  from Gaussian broadening of the transitions with  $\sigma = 2500 \text{ cm}^{-1}$ .

ligand-field transitions, for reasons that are discussed in Ref. [57].

In the experimental study, the very weak negative band and the weakly intense shoulder below and above  $15 \times 10^3 \text{ cm}^{-1}$  were assigned to the  $T_2$  and  $T_1$  triplet excited states, respectively. Nonrelativistic or scalar relativistic calculations do not give intensity at these energies. As seen in Figure 2, the 2c-TDDFT TDA PBE0 spectrum including both spin and orbital angular momentum contributions to the magnetic transition dipole moments (blue curve, labeled 'Spin') is essentially spot-on with the experiment, in terms of peak positions as well as in terms of the relative intensities of the triplet versus the singlet transitions. Very importantly, the signs of the rotatory strengths match the signs of the experimental bands. As can be seen in Figure 2, with the chosen broadening, the resulting absolute intensities and peak heights also match the experiment well, both for spin-allowed and spin-forbidden transitions.

Calculations were also performed without electron spin contributions in the magnetic moment operator  $\hat{m}$ , that is, only using the orbital angular momentum. The latter is the only source of rotatory strength in nonrelativistic and scalar relativistic calculations. It can be seen in Figure 2 that the intensity and band peak positions for the triplet excitations are sensitive to the electron spin contributions in the rotatory strength. Noticeably better agreement between the broadened calculated and the experimental spectrum is obtained when they are included. It is worth mentioning in this context that the peak positions for the triplet as well as the singlet  $E_g$  and  $A_2$  pair of bands do not coincide with the excitation energies, as demonstrated by the 'stick spectrum' in the right panel of Figure 2. The narrowly split  $T_1$  level with opposite rotatory strengths for  $E_g$  and  $A_2$  creates bands with peaks below and above the transition energies, with peak energies or wave-numbers that depend on the rotatory strengths, the transition energy splitting, and the chosen broadening. Differences in the

rotatory strengths are responsible for the different positions of the resolved low-energy  ${}^3E_g$  peak in the calculation without versus with electron spin contributions in the rotatory strength.

### Iridium NHC-helicene complexes and platinahelicenes

Table 1 summarizes the experimental and calculated emission data for the Ir(III) and Pt(II) systems of Figure 1. The experimentally reported energies correspond to the resolved vibronic peak positions. Compared to the highest experimental values, the 2c-TDDFT TDA PBE0 vertical transition energies underestimate the experiments consistently by a few tenth of an eV. Given that the decay rate constant  $k$ , Equation (3), contains a factor  $E^3$  (one power of  $E$  is from the oscillator strength), a small underestimation of  $E$  may translate into a significant underestimation of  $k$  and thus overestimated phosphorescence lifetime values. This is indeed what the calculations give.

Using full 2c-TDDFT, that is, without the TDA, led to a stronger underestimation of the transition energies (by an additional 0.2 eV for the platinahelicenes, 0.4 eV for Ir systems  $A^{1/2}$ , and less than 0.1 eV for  $\Lambda_{\text{Ir}}-A$ ; Table S2 in the Supporting Information). The full 2c-TDDFT calculations allowed for an assessment of dipole-length versus dipole-velocity data, which overall gave reasonable agreement (Table S2). We therefore consider the dipole-length results from the 2c-TDDFT TDA calculations to be reliable (see the Computational Section for further details). In the complete basis set limit, the two versions for the electric transition dipole become equivalent, and the length-gauge rotatory strength becomes origin-invariant. In practical calculations, that is, with finite basis sets, absent the use of a distributed gauge origin method such as gauge-including atomic orbitals,<sup>[64]</sup> the length-gauge results are origin dependent but typically reliable when the molecules are not far displaced from the origin.<sup>[37]</sup> The velocity gauge rotatory

**Table 1.** Experimental and calculated photophysical data for the Ir and Pt systems of Figure 1.<sup>[a]</sup>

|   | $(P, \Lambda_{\text{Ir}})-A^1$ | $(P, \Lambda_{\text{Ir}})-A^2$ | $\Lambda_{\text{Ir}}-A$   | P-3 a                      | P-3 c                  |
|---|--------------------------------|--------------------------------|---------------------------|----------------------------|------------------------|
| Experimental data   |                                |                                |                           |                            |                        |
| $E$ [eV]  | 2.36                           | 2.36                           |                           |                            |                        |
|   | 2.21                           | 2.21                           | 2.49                      | 1.91                       | 1.93                   |
|   | 2.04                           | 2.04                           |                           |                            |                        |
| $\tau$ [ $\mu\text{s}$ ]  | 350                            | 280                            | 0.53 / 2.4 <sup>[b]</sup> | 16.5                       | 21                     |
| $g_{\text{lum}}$  | $3.7 \times 10^{-3}$           | $1.5 \times 10^{-3}$           | $-9 \times 10^{-4}$       | $4.0 \times 10^{-3}$       | $3 \times 10^{-3}$     |
|   | (530)                          | (530)                          | (493)                     | ( $\lambda_{\text{max}}$ ) | (635) <sup>[c]</sup>   |
| Calculated TDDFT TDA PBE0 data  |                                |                                |                           |                            |                        |
| $E$ [eV] <sup>[d]</sup>   | 2.22                           | 2.22                           | 2.37                      | 1.76                       | 1.79                   |
| $\tau$ [ $\mu\text{s}$ ]  | 452                            | 417                            | 3.9                       | 92.7                       | 69.3                   |
| $g_{\text{lum}}$  | $8.12 \times 10^{-5}$          | $2.07 \times 10^{-3}$          | $-1.08 \times 10^{-3}$    | $-7.54 \times 10^{-4}$     | $-7.20 \times 10^{-4}$ |
| No spin   |                                |                                |                           |                            |                        |
| $g_{\text{lum}}$  | $1.24 \times 10^{-3}$          | $2.81 \times 10^{-3}$          | $-1.46 \times 10^{-3}$    | $2.21 \times 10^{-3}$      | $1.80 \times 10^{-3}$  |
| With Spin   |                                |                                |                           |                            |                        |
| [a] Measurements at room temperature. Values in parentheses below $g_{\text{lum}}$ data are the wavelengths in nm at which the dissymmetry factors were measured. Calculations for 298 K using $T_1$ equilibrium structures from TDDFT TDA PBE0 geometry optimization (see Tables S11 to S15 for the corresponding xyz coordinates). Calculated $g_{\text{lum}}$ from Equation (2). Results obtained with the spin-unrestricted DFT optimized structures are collected in Table S1. Experimental data for $(P, \Lambda_{\text{Ir}})-A^1$ , $(P, \Lambda_{\text{Ir}})-A^2$ , and $\Lambda_{\text{Ir}}-A$ taken from Ref. [23]. Experimental data for P-3 a and P-3 c taken from Ref. [30]. Vibronic peak positions provided for the $T_1-S_0$ emission where resolved. [b] Observed decay kinetics was bi-exponential at room-temperature. [c] Measured in dichloromethane solution with a CPL spectrofluorometer constructed in the laboratory at CNRS. The value of +0.013 reported for P-3 c in Ref. [30] is likely to be too high. [d] Vertical $T_1-S_0$ energies. ZFS was negligible for $(P, \Lambda_{\text{Ir}})-A^1$ and $(P, \Lambda_{\text{Ir}})-A^2$ . The individual triplet component energies (in eV) for the other systems were as follows: $\Lambda_{\text{Ir}}-A$ 2.36650, 2.36696, 2.37565; P-3 a 1.76391, 1.76409, 1.76445; P-3 c 1.79208, 1.79224, 1.79251. |                                |                                |                           |                            |                        |

strength is origin-invariant by construction, but results may differ considerably from the length gauge for commonly used basis sets. We focus on the dipole-length data from the TDA calculations in the remainder of the discussion.

A comparison of the results in Table 1 and Table S1 shows that the calculated emission data are not insensitive to the excited-state structures, but qualitatively the trends between the different sets of calculations and the experiments compare well: At room temperature,  $\tau$  is several hundred  $\mu\text{s}$  for the diastereoisomeric pair of the helicene-NHC cycloiridiated complexes ( $P, \Lambda_{\text{Ir}}\text{-A}^1$  and  $(P, \Delta_{\text{Ir}})\text{-A}^2$ , only a few  $\mu\text{s}$  for its corresponding model NHC system lacking the helicene unit  $\Lambda_{\text{Ir}}\text{-A}$ , and a few ten  $\mu\text{s}$  for the Pt-[8]helicene  $P\text{-3a}$  and Pt-[6]helicene  $P\text{-3c}$ . The calculations give noticeably too large lifetimes for  $P\text{-3a}$  and  $P\text{-3c}$ , but correctly identify them to be much smaller than those of  $(P, \Lambda_{\text{Ir}})\text{-A}^1$  and  $(P, \Delta_{\text{Ir}})\text{-A}^2$ . The large increase in the emission lifetime observed for the helicene-based iridium complexes, compared to the non-helicenic model, agrees well with the character of their  $T_1$  excited state, which for the former is strongly delocalized across the  $\pi$ -helical ligand and demonstrates the reduced contribution of the metal orbitals in the emission transition.<sup>[23]</sup>

The calculated  $g_{\text{lum}}$  (including electron spin contributions) are within a factor of two from the experimental estimates [within a factor of 3 for  $(P, \Lambda_{\text{Ir}})\text{-A}^1$ ], which can be considered satisfactory. The electron spin contributions in the magnetic transition dipole are seen to be very important for  $(P, \Lambda_{\text{Ir}})\text{-A}^1$ , raising  $g_{\text{lum}}$  by more than a factor of 10. For the platinahelicenes, the electron spin contributions are critical, because without them the rotatory strengths do not have the correct signs. Reference [30] previously reported  $g_{\text{lum}} = +0.013$ , much larger than the computed value. However, a revised experimental  $g_{\text{lum}}$  of  $+0.003$  is close to what we calculate.

It is important to note that for the iridium complexes, the computations (both with and without the electron spin contributions in the rotatory strength) reproduce correctly the trend in sign of measured  $g_{\text{lum}}$  for  $(P, \Lambda_{\text{Ir}})\text{-A}^1$  and  $(P, \Delta_{\text{Ir}})\text{-A}^2$  (positive) versus  $\Lambda_{\text{Ir}}\text{-A}$  (negative). This supports the finding drawn from the experimental data that the sign of the CPL signal of  $\text{A}^{1,2}$  is controlled by the stereochemistry of the  $\pi$ -helical NHC ligand, rather than stereochemistry at the metal.<sup>[23]</sup> For the platinahelicenes, the sign of  $g_{\text{lum}}$  also follows the stereochemistry of the helicene unit ( $P$  – positive,  $M$  – negative). However, the Pt center, because it is part of the helicene, participates more directly in the helical  $\pi$ -chromophore.<sup>[30]</sup> This is likely one of the main reasons why the sign of  $g_{\text{lum}}$  is not correctly predicted by the calculations that do not incorporate the electron spin in the magnetic transition dipole moment.

## Conclusion

The calculation of magnetic transition dipole moments, rotatory strengths, and velocity-gauge electric transition dipole moments was implemented in the two-component relativistic TDDFT module of the ADF package. The functionality will be available in the next release of ADF. Relativistic effects are

treated in the computations via the all-electron ZORA quasi-relativistic Hamiltonian, and they enter the associated frequency-dependent linear response to determine excitation energies and transition moments. The circular dichroism of the spin-forbidden and spin-allowed ligand-field transitions of tris(ethylenediamine)cobalt(III) modeled in this way agreed very well with measurements by Mason and Peart.<sup>[54]</sup> Phosphorescence dissymmetry factors  $g_{\text{lum}}$  and the corresponding lifetimes were calculated for three iridium complexes bearing helicenic or non-helicenic N-heterocyclic-carbene ligand and for two platinahelicenes. The agreement with experimental data was overall satisfactory, showing promise for future applications of the methodology to similar systems.<sup>[65,66]</sup> The calculations reproduced the signs and order of magnitude of  $g_{\text{lum}}$ , and the large variations of phosphorescence lifetimes among the complexes. The role of the electron spin contributions to the magnetic transition dipole moment was shown to be very important for one of the Ir systems and both platinahelicenes. For the latter,  $g_{\text{lum}}$  had the wrong sign when the electron spin contributions were not considered. Even for the cobalt complex, which exhibits comparatively smaller relativistic effects because of the lower nuclear charge of the metal, the electron spin contributions improved the appearance of the spin-forbidden ECD in comparison with the experimental spectrum. Further improvements of the calculations will likely be obtained by treating vibronic effects in the spectra. Work along these lines is being pursued in our laboratory.

## Computational Section

Triplet excited-state structures for the Ir and Pt complexes of Figure 1 were optimized with scalar ZORA spin-unrestricted DFT. Calculations used the PBE0<sup>[67]</sup> hybrid functional (25% global exact exchange) along with the TZ2P basis for the metal, DZ for hydrogens, and DZP otherwise, for optimizations and TDDFT runs, and employed a continuum solvent model with the dielectric constant for dichloromethane.<sup>[68]</sup> TDDFT response computations were based on the  $S_0$  closed-shell ground state at the  $T_1$  equilibrium structure, using spin-orbit ZORA and the 2c-TDDFT module with the 'FullKernel' option to determine the vertical transition energies and transition moments needed in Equations (1)–(3). The TDDFT calculations employed the Tamm-Dancoff approximation (TDA).<sup>[69]</sup> In agreement with observations made previously by Peach et al.,<sup>[70]</sup> and confirmed by us for some helicene-based metal complexes,<sup>[30,71,72]</sup> computations not employing the TDA underestimated the  $T_1$  energies significantly. The calculated total energy differences between the  $S_0$  and  $T_1$  states at the spin-unrestricted DFT-optimized  $T_1$  equilibrium structures likewise underestimated the emission energies substantially. Accordingly, an alternate set of  $T_1$  equilibrium structures was determined by TDDFT TDA PBE0 optimizations, using the Gaussian 09 program, revision D.03,<sup>[73]</sup> and def2-SV(P) Gaussian-type basis sets<sup>[74]</sup> with matching scalar relativistic effective core potentials for Ir and Pt. These structures were used for the 2c-TDDFT calculations reported herein. For completeness, results obtained with the spin-unrestricted DFT optimized  $T_1$  structures are provided in the Supporting Information, Table S1. In the present implementation, velocity gauge rotatory strengths are not available in conjunction with the TDA. Extensive test calculations with full TDDFT, in one- or two-component form, as documented in Section S2 in the Supporting Information for the cobalt complex, showed good agreement between the length and

velocity gauges for center-of-nuclear-charge (CNC) coordinates, and demonstrate the desired origin-invariance of the velocity-gauge results. To minimize errors from the origin dependence of the dipole-length gauge rotatory strengths in the TDA calculations, molecules were therefore placed at the CNC. Test calculations for *P-3c* with the platinum atom versus CNC at the coordinate origin (Tables S3 and S4 in the Supporting Information) showed that, while there is an origin dependence, it does not qualitatively affect the conclusions.

In reference to an actual or approximate (depending on the conformer) 3-fold rotational axis of symmetry of tris(ethylenediamine)cobalt(III), the C–C backbone of the ligand can either be approximately parallel (*le*) or oblique (*ob*), giving rise to 4 conformers for each of the  $\Delta$  and  $\Lambda$  configurations: *le*<sub>1</sub>, *le*<sub>2</sub>*ob*<sub>1</sub>, *le*<sub>1</sub>*ob*<sub>2</sub>, and *ob*<sub>3</sub>. The conformers structures of the complex [Co(en)<sub>3</sub>]<sup>3+</sup> were optimized with three different functionals, namely BP86,<sup>[75,76]</sup> B3LYP,<sup>[77,78]</sup> and PBE0, to examine the sensitivity of the calculated spectrum to the underlying structural parameters. The [Co(en)<sub>3</sub>]<sup>3+</sup> spectra were simulated using the same set of functionals, with and without the TDA. In all these computations the aforementioned basis set combination (TZ2P/DZP/DZ) was used and a continuum solvent model (COSMO) was employed to simulate solvent (water) effects. With the B3LYP functional, the different conformers were within less than 1 kcal/mol in energy and therefore the calculations do not reliably identify a most abundant conformer, in agreement with NMR studies.<sup>[79,80]</sup> In agreement with Ref. [63], solvent effects on the ligand-field transition were weak. Moreover, the ligand-field ECD spectra for the different conformers were very similar, and the underlying dependence of the spectra on the functional used for the structure optimizations was weak. In agreement with Ref. [57], the PBE0 functional performed best for the spectrum. TDA calculations showed a marked improvement of the triplet excitations. For all these reasons, most of the data computed for  $\Lambda$ -[Co(en)<sub>3</sub>]<sup>3+</sup> are collected in the Supporting Information, and we focus the discussion on the gas-phase TDA PBE0 spectrum of the B3LYP-optimized *le*<sub>3</sub> conformer. Note that *le*<sub>3</sub> is the conformer adopted in crystals containing the complex on which ECD measurements were carried out previously.<sup>[54]</sup>

## Acknowledgements

We acknowledge the Center for Computational Research (CCR)<sup>[81]</sup> at the University at Buffalo for providing computational resources. This study has been supported by grant CHE-1855470 from the National Science Foundation. J.C. warmly thanks Debsouri Kundu and Dr. Natalia Del Rio for the measurement of the CPL spectrum of complex *P-3c* using a locally assembled JASCO CPL spectrometer. J.A. and H.D.L. would like to thank Dr. Barry Moore II for implementing the orbital angular momentum component of the magnetic transition moment in the SO-TDDFT code during the course of his PhD research.

## Conflict of Interest

The authors declare no conflict of interest.

## Data Availability Statement

The data that support the findings of this study are available from the corresponding author upon reasonable request.

**Keywords:** optical activity · spin-forbidden transitions · luminescence · helicenes · time-dependent density functional theory

- [1] H. Yersin, Ed., *Highly Efficient OLEDs with Phosphorescent Materials*, John Wiley & Sons, 2007.
- [2] L. F. Gildea, J. A. G. Williams, in *Organic Light-Emitting Diodes (OLEDs)* (Ed.: A. Buckley), Woodhead Publishing, 2013, pp. 77–113.
- [3] N. Armaroli, H. J. Bolink, Eds., *Photoluminescent Materials and Electroluminescent Devices*, Springer, 2017.
- [4] E. Longhi, L. De Cola, in *Iridium(III) in Optoelectronic and Photonics Applications*, John Wiley & Sons, Ltd, 2017, pp. 205–274.
- [5] T. Sajoto, P. I. Djurovich, A. B. Tamayo, J. Oxgaard, W. A. Goddard, M. E. Thompson, *J. Am. Chem. Soc.* **2009**, *131*, 9813–9822.
- [6] T. Hofbeck, H. Yersin, *Inorg. Chem.* **2010**, *49*, 9290–9299.
- [7] T. Matsushita, T. Asada, S. Koseki, *J. Phys. Chem. C* **2007**, *111*, 6897–6903.
- [8] E. Jansson, B. Minaev, S. Schrader, H. Ågren, *Chem. Phys.* **2007**, *333*, 157–167.
- [9] J. M. Younker, K. D. Dobbs, *J. Phys. Chem. C* **2013**, *117*, 25714–25723.
- [10] K. Mori, T. P. M. Goumans, E. van Lenthe, F. Wang, *Phys. Chem. Chem. Phys.* **2014**, *16*, 14523–14530.
- [11] M. Kühn, F. Weigend, *J. Chem. Phys.* **2015**, *142*, 034116.
- [12] M. Kleinschmidt, C. van Wüllen, C. M. Marian, *J. Chem. Phys.* **2015**, *142*, 094301.
- [13] D. Escudero, *Chem. Sci.* **2016**, *7*, 1262–1267.
- [14] X. Zhang, D. Jacquemin, Q. Peng, Z. Shuai, D. Escudero, *J. Phys. Chem. C* **2018**, *122*, 6340–6347.
- [15] R. Feng, X. Yu, J. Autschbach, *J. Chem. Theory Comput.* **2021**, *17*, 7531–7544.
- [16] Y. Yang, R. C. da Costa, D. M. Smilgies, A. J. Campbell, M. J. Fuchter, *Adv. Mater.* **2013**, *25*, 2624–2628.
- [17] J. R. Brandt, X. Wang, Y. Yang, A. J. Campbell, M. J. Fuchter, *J. Am. Chem. Soc.* **2016**, *138*, 9743–9746.
- [18] K. Dhbaibi, L. Abella, S. Meunier-Della-Gatta, T. Roisnel, N. Vanthuyne, B. Jamoussi, G. Pieters, B. Racine, E. Quesnel, J. Autschbach, J. Crassous, L. Favereau, *Chem. Sci.* **2021**, *12*, 5522–5533.
- [19] S. Kasemthaveechok, L. Abella, M. Jean, M. Cordier, T. Roisnel, N. Vanthuyne, T. Guizouarn, O. Cador, J. Autschbach, J. Crassous, L. Favereau, *J. Am. Chem. Soc.* **2020**, *142*, 20409–20418.
- [20] N. Saleh, C. Shen, J. Crassous, *Chem. Sci.* **2014**, *5*, 3680–3694.
- [21] J. OuYang, J. Crassous, *Coord. Chem. Rev.* **2018**, *376*, 533–547.
- [22] M. Srebro-Hooper, J. Crassous, J. Autschbach, in *Helicenes: From Synthesis to Properties and Applications* (Eds.: I. Stary, I. Stara, J. Crassous), Wiley-VCH, Weinheim, in press.
- [23] N. Hellou, M. Srebro-Hooper, L. Favereau, F. Zinna, E. Caytan, L. Toupet, V. Dorcet, M. Jean, N. Vanthuyne, A. G. Williams, L. Di Bari, J. Autschbach, J. Crassous, *Angew. Chem. Int. Ed.* **2017**, *56*, 8236–8239; *Angew. Chem.* **2017**, *129*, 8348–8351.
- [24] L. Zhang, E. Meggers, *Acc. Chem. Res.* **2017**, *50*, 320–330.
- [25] R. Gao, D. G. Ho, B. Hernandez, M. Selke, D. Murphy, P. I. Djurovich, M. E. Thompson, *J. Am. Chem. Soc.* **2002**, *124*, 14828–14829.
- [26] S. C. J. Meskers, H. P. J. M. Dekkers, *Spectrochim. Acta Part A* **1999**, *55*, 1857–1874.
- [27] L. Norel, M. Rudolph, N. Vanthuyne, J. A. G. Williams, C. Lescop, C. Roussel, J. Autschbach, J. Crassous, R. Réau, *Angew. Chem. Int. Ed.* **2010**, *49*, 99–102; *Angew. Chem.* **2010**, *122*, 103–106.
- [28] E. Anger, M. Rudolph, L. Norel, S. Zrig, C. Shen, N. Vanthuyne, L. Toupet, J. A. G. Williams, C. Roussel, J. Autschbach, J. Crassous, R. Réau, *Chem. Eur. J.* **2011**, *17*, 14178–14198.
- [29] C. Shen, E. Anger, M. Srebro, N. Vanthuyne, L. Toupet, C. Roussel, J. Autschbach, R. Réau, J. Crassous, *Chem. Eur. J.* **2013**, *19*, 16722–16728.
- [30] C. Shen, E. Anger, M. Srebro, N. Vanthuyne, K. K. Deol, T. D. Jefferson, G. Muller, J. A. G. Williams, L. Toupet, C. Roussel, J. Autschbach, R. Réau, J. Crassous, *Chem. Sci.* **2014**, *5*, 1915–1927.

- [31] N. Saleh, B. Moore II, M. Srebro, N. Vanthuyne, L. Toupet, J. A. G. Williams, C. Roussel, K. K. Deol, G. Muller, J. Autschbach, J. Crassous, *Chem. Eur. J.* **2015**, *21*, 1673–1681.
- [32] C. Shen, M. Srebro-Hooper, M. Jean, N. Vanthuyne, L. Toupet, J. A. G. Williams, A. R. Torres, A. J. Riives, G. Muller, J. Autschbach, J. Crassous, *Chem. Eur. J.* **2017**, *23*, 407–418.
- [33] a) J. Autschbach, *J. Chem. Phys.* **2012**, *136*, 150902; b) M. Barysz, Y. Ishikawa (editors), *Relativistic Methods for Chemists*, Vol. 10 of Challenges and Advances in Computational Chemistry and Physics, Springer, Dordrecht, **2010**.
- [34] B. O. Roos, R. Lindh, P. Å. Malmqvist, V. Verazov, P.-O. Widmark, *Multiconfigurational Quantum Chemistry*, John Wiley & Sons, Hoboken, NJ, **2016**.
- [35] F. Neese, *Wiley Interdiscip. Rev.: Comput. Mol. Sci.* **2018**, *8*, e1327.
- [36] F. Aquilante, J. Autschbach, A. Baiardi, S. Battaglia, V. A. Borin, L. F. Chibotaru, I. Conti, L. De Vico, M. Delcey, I. Fdez. Galván, N. Ferré, L. Freitag, M. Garavelli, X. Gong, S. Knecht, E. D. Larsson, R. Lindh, M. Lundberg, P. Å. Malmqvist, A. Nenov, J. Norell, M. Odellius, M. Olivucci, T. B. Pedersen, L. Pedraza-González, Q. M. Phung, K. Pierloot, M. Reiher, I. Schapiro, J. Segarra-Martí, F. Segatta, L. Seijo, S. Sen, D.-C. Sergentu, C. J. Stein, L. Ungur, M. Vacher, A. Valentini, V. Veryazov, *J. Chem. Phys.* **2020**, *152*, 214117.
- [37] F. Gendron, B. Moore II, O. Cador, F. Pointillart, J. Autschbach, B. Le Guennic, *J. Chem. Theory Comput.* **2019**, *15*, 4140–4155.
- [38] C. Badala Viswanatha, B. Helmich-Paris, C. Hättig, *Phys. Chem. Chem. Phys.* **2018**, *20*, 21051–21061.
- [39] D. Rappoport, F. Furche, in *Time-Dependent Density Functional Theory* (Eds.: M. A. L. Marques, C. A. Ullrich, F. Nogueira, A. Rubio, K. Burke, E. K. U. Gross), Springer, Berlin, **2006**.
- [40] P. Elliott, K. Burke, F. Furche, in *Reviews of Computational Chemistry* (Eds.: K. B. Lipkowitz, T. R. Cundari), Wiley, Hoboken, NJ, **2009**.
- [41] T. Saue, H. J. Aa. Jensen, *J. Chem. Phys.* **2003**, *118*, 522–536.
- [42] E. Jansson, P. Norman, B. Minaev, H. Ågren, *J. Chem. Phys.* **2006**, *124*, 114106.
- [43] J. Autschbach, L. Nitsch-Velasquez, M. Rudolph, *Top. Curr. Chem.* **2011**, *298*, 1–98.
- [44] M. Srebro-Hooper, J. Autschbach, *Annu. Rev. Phys. Chem.* **2017**, *68*, 399–420.
- [45] G. Longhi, E. Castiglioni, J. Koshoubu, G. Mazzeo, S. Abbate, *Chirality* **2016**, *28*, 696–707.
- [46] B. Pritchard, J. Autschbach, *ChemPhysChem* **2010**, *11*, 2409–2415.
- [47] S. Grimme, *J. Chem. Phys.* **2013**, *138*, 244104.
- [48] C. Bannwarth, S. Grimme, *Comput. Theor. Chem.* **2014**, *1040–1041*, 45–53.
- [49] Q. Yang, M. Fusè, J. Bloino, V. Barone, *Spectrochim. Acta Part A* **2021**, *254*, 119631.
- [50] M. Kamiński, J. Cukras, M. Pecul, A. Rizzo, S. Coriani, *Phys. Chem. Chem. Phys.* **2015**, *17*, 19079–19086.
- [51] F. Wang, T. Ziegler, E. Van Lenthe, S. Van Gisbergen, E. J. Baerends, *J. Chem. Phys.* **2005**, *122*, 204103–12.
- [52] M. Kühn, F. Weigend, *J. Chem. Phys.* **2014**, *141*, 224302.
- [53] F. Egidi, M. Fusè, A. Baiardi, J. Bloino, X. Li, V. Barone, *Chirality* **2018**, *30*, 850–865.
- [54] S. F. Mason, B. J. Peart, *J. Chem. Soc. Dalton Trans.* **1977**, 937.
- [55] J. Autschbach, T. Ziegler, S. J. A. van Gisbergen, E. J. Baerends, *J. Chem. Phys.* **2002**, *116*, 6930–6940.
- [56] F. E. Jorge, J. Autschbach, T. Ziegler, *J. Am. Chem. Soc.* **2005**, *127*, 975–985.
- [57] M. Rudolph, T. Ziegler, J. Autschbach, *Chem. Phys.* **2011**, *391*, 92–100.
- [58] E. J. Baerends, T. Ziegler, A. J. Atkins, J. Autschbach, D. Bashford, O. Baseggio, A. Bérces, F. M. Bickelhaupt, C. Bo, P. M. Boerrigter, L. Cavallo, C. Daul, D. P. Chong, D. V. Chulhai, L. Deng, R. M. Dickson, J. M. Dieterich, D. E. Ellis, M. van Faassen, L. Fan, T. H. Fischer, C. Fonseca Guerra, M. Franchini, A. Ghysels, A. Giammona, S. J. A. van Gisbergen, A. Goetz, A. W. Götz, J. A. Groeneveld, O. V. Gritsenko, M. Grüning, S. Gusarov, F. E. Harris, P. van den Hoek, Z. Hu, C. R. Jacob, H. Jacobsen, L. Jensen, L. Joubert, J. W. Kaminski, G. van Kessel, C. König, F. Kootstra, A. Kovalenko, M. V. Krykunov, E. van Lenthe, D. A. McCormack, A. Michalak, M. Mitoraj, S. M. Morton, J. Neugebauer, V. P. Nicu, L. Noodleman, V. P. Osinga, S. Patchkovskii, M. Pavanello, C. A. Peebles, P. H. T. Philipsen, D. Post, C. C. Pye, H. Ramanantoanina, P. Ramos, W. Ravenek, J. I. Rodríguez, P. Ros, R. Rüger, P. R. T. Schipper, D. Schlüns, H. van Schoot, G. Schreckenbach, J. S. Seldenthuis, M. Seth, J. G. Snijders, M. Solà, M. Stener, M. Swart, D. Swerhone, V. Tognetti, G. te Velde, P. Vernooijs, L. Versluis, L. Visscher, O. Visser, F. Wang, T. A. Wesolowski, E. M. van Wezenbeek, G. Wiesenekker, S. K. Wolff, T. K. Woo, A. L. Yakovlev, ADF version 2019.3, SCM, Theoretical Chemistry, Vrije Universiteit, Amsterdam, the Netherlands.
- [59] E. van Lenthe, E. J. Baerends, J. G. Snijders, *J. Chem. Phys.* **1993**, *99*, 4597–4610.
- [60] E. van Lenthe, E. J. Baerends, *J. Comput. Chem.* **2003**, *24*, 1142–1156.
- [61] S. J. A. van Gisbergen, J. G. Snijders, E. J. Baerends, *Comput. Phys. Commun.* **1999**, *118*, 119–138.
- [62] O. Kahn, *Molecular Magnetism*, VCH, New York, **1993**.
- [63] J. Autschbach, F. E. Jorge, T. Ziegler, *Inorg. Chem.* **2003**, *42*, 2867–2877.
- [64] J. Autschbach, *ChemPhysChem* **2011**, *12*, 3224–3235.
- [65] A. Macé, N. Hellou, J. Hammoud, C. Martin, E. S. Gauthier, L. Favereau, T. Roisnel, E. Caytan, G. Nasser, N. Vanthuyne, J. A. G. Williams, F. Berrée, B. Carboni, J. Crassous, *Helv. Chim. Acta* **2019**, *102*, e1900044.
- [66] E. S. Gauthier, N. Hellou, E. Caytan, S. Del Fré, V. Dorcet, N. Vanthuyne, L. Favereau, M. Srebro-Hooper, J. A. G. Williams, J. Crassous, *Inorg. Chem. Front.* **2021**, *8*, 3916–3925.
- [67] C. Adamo, V. Barone, *J. Chem. Phys.* **1999**, *110*, 6158–6170.
- [68] C. C. Pye, T. Ziegler, *Theor. Chem. Acc.* **1999**, *101*, 396–408.
- [69] S. Hirata, M. Head-Gordon, *Chem. Phys. Lett.* **1999**, *314*, 291–299.
- [70] M. J. G. Peach, M. J. Williamson, D. J. Tozer, *J. Chem. Theory Comput.* **2011**, *7*, 3578–3585.
- [71] E. Anger, M. Srebro, N. Vanthuyne, C. Roussel, L. Toupet, J. Autschbach, R. Réau, J. Crassous, *Chem. Commun.* **2014**, *50*, 2854–2856.
- [72] N. Saleh, M. Srebro, T. Reynaldo, N. Vanthuyne, L. Toupet, V. Y. Chang, G. Muller, J. A. G. Williams, C. Roussel, J. Autschbach, J. Crassous, *Chem. Commun.* **2015**, *51*, 3754–3757.
- [73] M. J. Frisch, G. W. Trucks, H. B. Schlegel, G. E. Scuseria, M. A. Robb, J. R. Cheeseman, G. Scalmani, V. Barone, G. A. Petersson, H. Nakatsuji, X. Li, M. Caricato, A. Marenich, J. Bloino, B. G. Janesko, R. Gomperts, B. Mennucci, H. P. Hratchian, J. V. Ortiz, A. F. Izmaylov, J. L. Sonnenberg, D. Williams-Young, F. Ding, F. Lipparini, F. Egidi, J. Goings, B. Peng, A. Petrone, T. Henderson, D. Ranasinghe, V. G. Zakrzewski, J. Gao, N. Rega, G. Zheng, W. Liang, M. Hada, M. Ehara, K. Toyota, R. Fukuda, J. Hasegawa, M. Ishida, T. Nakajima, Y. Honda, O. Kitao, H. Nakai, T. Vreven, K. Throssell, J. A. Montgomery, Jr., J. E. Peralta, F. Ogliaro, M. Bearpark, J. J. Heyd, E. Brothers, K. N. Kudin, V. N. Staroverov, T. Keith, R. Kobayashi, J. Normand, K. Raghavachari, A. Rendell, J. C. Burant, S. S. Iyengar, J. Tomasi, M. Cossi, J. M. Millam, M. Klene, C. Adamo, R. Cammi, J. W. Ochterski, R. L. Martin, K. Morokuma, O. Farkas, J. B. Foresman, D. J. Fox, Gaussian 09, Revision D.01, Gaussian, Inc., Wallingford CT, 2009.
- [74] F. Weigend, R. Ahlrichs, *Phys. Chem. Chem. Phys.* **2005**, *7*, 3295–3305.
- [75] A. D. Becke, *Phys. Rev. A* **1988**, *38*, 3098–3100.
- [76] J. P. Perdew, *Phys. Rev. B* **1986**, *33*, 8822–8824.
- [77] A. D. Becke, *J. Chem. Phys.* **1993**, *98*, 5648–5652.
- [78] C. Lee, W. Yang, R. G. Parr, *Phys. Rev. B* **1988**, *37*, 785–789.
- [79] R. Kuroda, Y. Saito, in *Circular Dichroism: Principles and Applications, Second Edition* (Eds.: N. Berova, K. Nakanishi, R. W. Woody), Wiley VCH, New York, **2000**, pp. 563–599.
- [80] J. K. Beattie, *Acc. Chem. Res.* **1971**, *4*, 253–259.
- [81] Center for Computational Research, University at Buffalo. URL <https://hdl.handle.net/10477/79221>. Accessed 04/2022.

Manuscript received: February 1, 2022

Revised manuscript received: May 4, 2022